Ferromagnetic resonance linewidth in metallic thin films: Comparison of measurement methods

Sangita S. Kalarickal,[a] Pavol Krivosik,[b] Mingzhong Wu, and Carl E. Patton
Department of Physics, Colorado State University, Fort Collins, Colorado 80523

Michael L. Schneider, Pavel Kabos, and T. J. Silva
National Institute of Standards and Technology, Boulder, Colorado 80305

John P. Nibarger
Sun Microsystems, One StorageTek Drive, Louisville, Colorado 80028

(Received 5 September 2005; accepted 21 March 2006; published online 15 May 2006)

Stripline (SL), vector network analyzer (VNA), and pulsed inductive microwave magnetometer (PIMM) techniques were used to measure the ferromagnetic resonance (FMR) linewidth for a series of Permalloy films with thicknesses of 50 and 100 nm. The SL-FMR measurements were made for fixed frequencies from 1.5 to 5.5 GHz. The VNA-FMR and PIMM measurements were made for fixed in-plane fields from 1.6 to 8 kA/m (20–100 Oe). The results provide a confirmation, lacking until now, that the linewidths measured by these three methods are consistent and compatible. In the field format, the linewidths are a linear function of frequency, with a slope that corresponds to a nominal Landau-Lifshitz phenomenological damping parameter α value of 0.007 and zero frequency intercepts in the 160–320 A/m (2–4 Oe) range. In the frequency format, the corresponding linewidth versus frequency response shows a weak upward curvature at the lowest measurement frequencies and a leveling off at high frequencies. © *2006 American Institute of Physics*. [DOI: 10.1063/1.2197087]

I. INTRODUCTION

Together with the areal density of hard disk data storage systems, the data transfer rate in magnetic recording systems has increased significantly over the past decade. Recent advances in magnetic film based memory devices hold great promise for fast, high density magnetic random access memory (MRAM) devices. The switching speed of the magnetic elements for these applications is limited, in part, by the magnetic damping in the thin film materials. An understanding of the damping mechanisms and control parameters remains one of the key challenges in the push to achieve faster switching speeds.

Broadly speaking, three techniques have been developed for the measurement of the ferromagnetic resonance (FMR) and the magnetodynamic damping parameters in metallic ferromagnetic thin films in the 1–10 GHz range of frequencies. The first is a stripline (SL) based FMR technique developed in the 1960s.[1] This is closely related to standard shortened waveguide[2,3] and microwave cavity[4] FMR measurement techniques where one measures the FMR linewidth by sweeping the field at a fixed frequency. The second utilizes a vector network analyzer (VNA) instrumentation, a swept frequency at a fixed field, and a conversion of the basic *S* parameters so obtained into FMR absorption curves and extracted linewidths.[5] The third involves the use of a pulsed inductive microwave magnetometry (PIMM).[6,7] This technique significantly extends an earlier work on the inductive detection of magnetization switching[8] through the use of modern, fast rise time drive electronics, coplanar waveguides for simultaneous drive and detection, and digital signal processing. The Fourier transform of the PIMM time domain response yields the FMR absorption profile in frequency and the corresponding linewidths.

The SL, VNA, and PIMM techniques all have advantages and disadvantages. All three are relatively broad bands. While the strip line approach is simple to run, the sensitivity is low. The VNA approach takes advantage of the full amplitude and phase analysis capabilities of advanced commercial vector network analyzer instruments. This approach, however, requires a careful calibration and the proper subtraction of reference signals in order to obtain accurate results. The advantages of the PIMM method lie in the use of a dc field step rather than a microwave excitation, time resolved magnetization decay data that correspond to a wide band FMR response in the frequency domain, and the absence of a complicated calibration procedure. As with the VNA approach, the main PIMM disadvantage is that the data analysis is extremely complicated, with the need for a careful subtraction of the background pulse.

In spite of the intensive metal film FMR work over many years, there has been no systematic comparison of the actual decay rates and linewidths that are obtained from these different methods. The purpose of this work was to measure decay rates and FMR linewidths for representative Permalloy thin films by all three techniques, analyze the data in a systematic way, and compare the results. These comparisons were made in terms of the conventional half power field swept linewidth from SL-FMR measurements and the frequency swept linewidth from VNA-FMR measurements and

[a]Electronic mail: sangita@lamar.colostate.edu
[b]On leave from the Department of Electromagnetic Field Theory, Faculty of Electrical Engineering and Information Technology, Bratislava, Slovakia.

PIMM fast Fourier transform (FFT) analyses. The results show that both formats provide consistent values of the damping and relaxation parameters for these films.

Section II describes the three loss measurement techniques. The section also gives a brief description of the samples used for the measurements. Section III outlines the procedures for conversions between field swept and frequency swept linewidths that are needed for a comparison of the various results. Section IV presents the experimental results and comparisons for the three methods.

II. SAMPLES AND MEASUREMENT METHODS: SL-FMR, VNA-FMR, AND PIMM TECHNIQUES

This section reviews the three techniques presented in the Introduction and describes the samples. In SL-FMR measurements, one varies the static magnetic field at a fixed microwave frequency, obtains a FMR absorption profile, and determines the half power field swept linewidth ΔH_{SL} as the full width at half maximum (FWHM) of the response. In VNA-FMR experiments, on the other hand, one varies the microwave frequency at a fixed static field, extracts the FMR absorption profile from standard S parameter measurements, and obtains a FWHM frequency swept linewidth Δf_{VNA} from the response. The PIMM technique departs significantly from these two approaches. Here, one applies an excitation magnetic field transverse to the fixed static field in the form of a step or an impulse, detects the ringing response of the dynamic magnetization $m(t)$, and performs a FFT analysis to convert the time domain response to an $m(\omega)$ response profile. An equivalent FWHM frequency swept linewidth Δf_{PIMM} is then extracted from this profile.

Standard field deposited Permalloy films with an in-plane uniaxial anisotropy were chosen for the comparison measurements because of their good soft magnetic properties and nominally low linewidths. The 80 at. % Ni and 20 at. % Fe films were prepared by standard sputtering techniques on 1×1 cm^2 glass substrates, with an initial 5 nm Ta seed layer. The films were deposited at room temperature with the substrates mounted on a rotating fixture with permanent magnets that provided a nominal in-plane field of 2 kA/m (25 Oe). Two 50 nm thick samples (S50A and S50B) and one 100 nm thick sample (S100) were fabricated for the data and results given below. Samples S50A and S100 were used for the SL-FMR and PIMM measurements. Sample S50B was used for the VNA-FMR measurements. A standard inductive hysteresis loop tracer was used to determine the coercive force and uniaxial anisotropy field of the films. The films had square easy direction and straight line hard direction hysteresis loops, with coercive forces and anisotropy fields in the 160 and 400 A/m (2 and 5 Oe) ranges, respectively.

A. The stripline ferromagnetic resonance technique

The stripline ferromagnetic resonance technique gives the user the flexibility to operate in a wide band of frequencies through the use of a nonresonant strip transmission line. This avoids the usual restricted bandwidths that result from conventional shortened waveguide or cavity methods. The broadband stripline FMR spectrometer used for the measurements shown below follows the design given in Ref. 1.

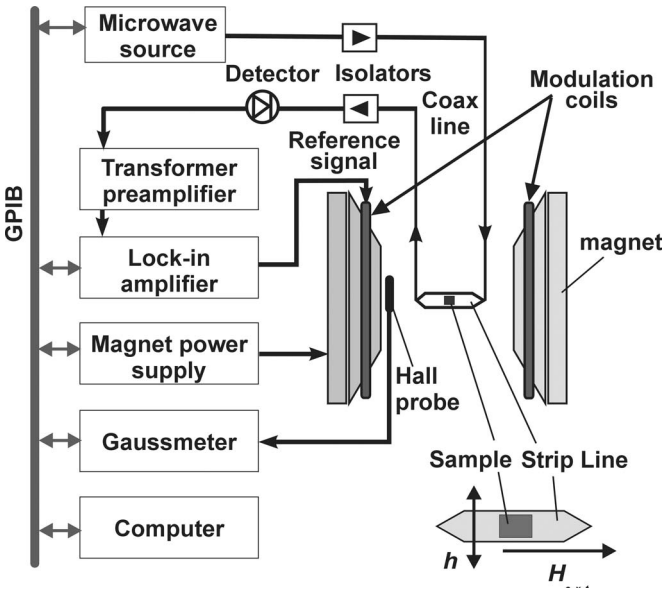

FIG. 1. Schematic diagram of the stripline ferromagnetic resonance spectrometer. The inset shows the field geometry and sample with respect to the strip transmission line. The sample is placed near one ground plane of the stripline structure and directly above the stripline. The mutually perpendicular static applied field H_{ext} and the microwave field h are both in the film plane, as indicated.

Figure 1 shows a schematic of the system. The spectrometer consists of a synthesized frequency sweeper as the continuous wave microwave input signal source, a double ground plane 50 Ω strip transmission line for a sample excitation, coaxial isolators for a voltage standing wave ratio (VSWR) reduction, and a Schottky diode for detection. Field modulation and a lock-in amplifier are used to extract the derivative of the absorbed power versus field profile. The inset in Fig. 1 shows the sample and the field geometry.

The sample was mounted flush with one ground plane of the stripline to ensure a reasonable homogeneity in the microwave field over the roughly 1 cm^2 sample area. The microwave input power was always kept below 1 mW to ensure a linear response. The static magnetic field was applied in the plane of the film, perpendicular to the microwave field and parallel to the easy axis of the sample.

The experimental FMR absorption derivative versus field profiles were generally undistorted and symmetric. A direct numerical integration of the data gave near Lorentzian profiles. The full width at half maximum of a Lorentzian fit to the integrated data was then used as a measure of the half power FMR linewidth of the film. The error in the linewidth determinations was typically below 80 A/m (1 Oe).

Figure 2 shows representative SL-FMR data for sample S50A. Figure 2(a) shows a typical measured absorption derivative versus field profile for a 3 GHz microwave excitation. The profile is symmetric and clean. The solid circles in Fig. 2(b) show the normalized integrated data, and the solid curve shows the Lorentzian fit. A resonance field H_{res} of 8.08 ± 0.04 kA/m (101 ± 0.5 Oe) and a half power linewidth ΔH_{SL} value of 1.5 ± 0.04 kA/m (18.3 ± 0.5 Oe) were obtained from these data.

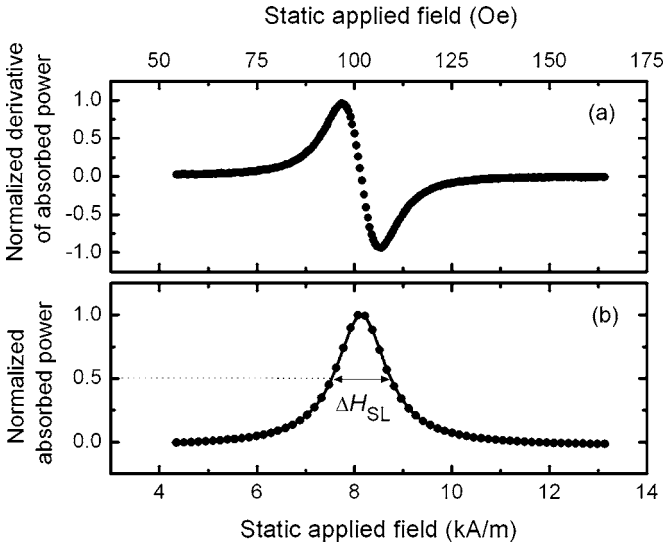

FIG. 2. Representative stripline ferromagnetic resonance (SL-FMR) data. Graph (a) shows ferromagnetic resonance absorption derivative vs static applied field data for film S50A at 3 GHz. Graph (b) shows the normalized integrated response from (a) as a function of field. The solid curve in (b) is a Lorentzian fit to the data.

B. The vector network analyzer ferromagnetic resonance technique

The VNA-FMR technique also allows for operation over a wide frequency band and yields FMR parameters from standard microwave *S*− parameter measurements versus frequency and field. Figure 3 shows a diagram of the system. The microwave drive in this case is provided by a coplanar waveguide (CPW) excitation structure, with the thin film sample positioned across the center conductor as indicated. The static magnetic field is provided by a set of Helmholtz coils. The signal analysis is done with a standard vector network analyzer.

The coplanar waveguide had a 100 μm wide center strip. The static field was applied in the plane of the film and perpendicular to the microwave field. The setup was then used to obtain the standard microwave *S* parameters as a function of frequency at a fixed field for the CPW line with the sample in place. Data were collected for a range of fixed static fields from 1.6 to 8.4 kA/m (20–106 Oe). A typical frequency sweep extended to 4.4 GHz. For sweeps at FMR

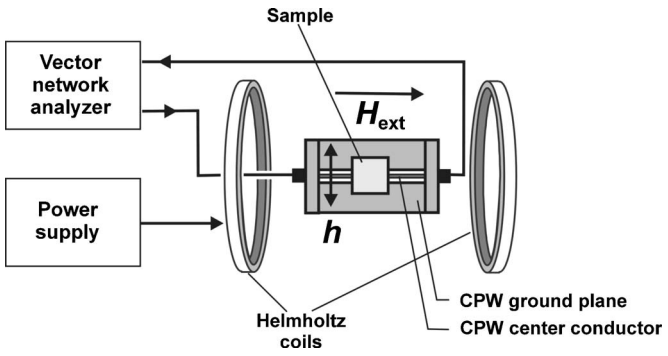

FIG. 3. Schematic diagram of the vector network analyzer ferromagnetic resonance spectrometer. The sample is placed on the coplanar waveguide (CPW) structure, as indicated. The mutually perpendicular static applied field H_{ext} and the microwave field *h* are in the plane of the film.

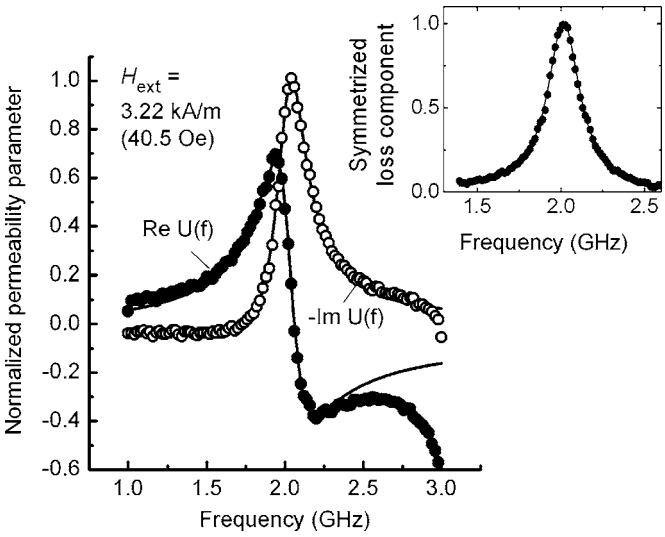

FIG. 4. Representative vector network analyzer ferromagnetic resonance (VNA-FMR) data that show the normalized permeability parameter *U* vs frequency *f* for film S50B at an static applied field H_{ext}=3.22 kA/m (40.5 Oe). The solid circles show the Re$[U(f)]$, and the open circles show the −Im$[U(f)]$ values extracted from the experimental *S* parameters. The solid curves show fits to the data. The inset shows the data in a normalized loss component format, with conversion based on the same fit parameters used to obtain the solid curves in the main figure plot. The solid curve in the inset shows the theoretical loss profile.

fields below 3.72 kA/m (46.7 Oe), the reference field was set at 8.40 kA/m (106 Oe), the maximum available field. For FMR fields above this midvalue of 3.72 kA/m, a low reference field value of 748 A/m (9.4 Oe), still sufficient to saturate the film, was used. As noted below, the proximity of the reference field to the measurement field can lead to problems in some cases.

The data were analyzed on the basis of a transmission line model developed by Barry[5] under the assumption that the dominant CPW mode was the TEM mode. If the effect of reflections is neglected, the Barry analysis gives an uncalibrated effective microwave permeability parameter of the form

$$U(f) = \pm \frac{i \ln[S_{21-\mathrm{H}}(f)/S_{21-\mathrm{ref}}(f)]}{\ln[S_{21-\mathrm{ref}}(f)]}, \tag{1}$$

where the sign is chosen to make Im$[U(f)]$ negative in the vicinity of the FMR peak. The *f* denotes the common set of frequency points for the two data runs, $S_{21-\mathrm{H}}(f)$ denotes the set of S_{21} parameters at the FMR field of interest, and $S_{21-\mathrm{ref}}(f)$ is the set of S_{21} parameters at the reference field. One needs both FMR data and reference data in order to calibrate out the response properties of the excitation structure, feed cables, etc., that do not relate to the FMR response. Under ideal circumstances, −Im$[U(f)]$ versus *f* would correspond to the FMR loss profile and Re$[U(f)]$ would show the dispersion. The $U(f)$ notation is used to emphasize that this raw measured response is related to the actual complex microwave permeability μ. Note that one obtains a full $U(f)$ data set for each measurement field of interest.

Figure 4 shows representative 1–3 GHz results for film S50B at H_{ext}=3.22 kA/m (40.5 Oe), with the reference data at H_{ext}=8.40 kA/m (106 Oe). The film was oriented with the

uniaxial anisotropy easy axis parallel to the CPW line. The open and solid circles show the data for $-\mathrm{Im}[U(f)]$ and $\mathrm{Re}[U(f)]$, respectively, with all data normalized to give a maximum $-\mathrm{Im}[U(f)]$ value of unity at the FMR peak. The solid curves show fits that will be discussed shortly. The main point of note is that the responses shown for $-\mathrm{Im}[U(f)]$ and $\mathrm{Re}[U(f)]$ do not correspond strictly to the loss and dispersion profiles expected from the FMR theory.[9] The $-\mathrm{Im}[U(f)]$ response is asymmetric and actually drops below zero at low frequencies. The $\mathrm{Re}[U(f)]$ response shows a significant departure from a dispersive response above about 2.3 GHz.

These distortions are attributed to two effects: (1) the neglect of reflections in the simplified analysis that gives Eq. (1) and (2) the proximity of the reference field value to the FMR field points. The result is a combination of offsets and distortions due to the FMR response embedded in the reference data as well as a mixing of the real and imaginary components of the actual susceptibility $\chi(f)$ in the measurements. Linewidths were obtained through an empirical scheme in which the data were fitted to a modified susceptibility response function of the form $\chi_0+\chi(f)e^{i\phi}$, where χ_0 is a complex offset parameter and ϕ is a phase shift. This procedure was applied for each of the measurement fields to obtain frequency linewidth Δf_{VNA} values versus the FMR frequency. Details are given below.

The complex susceptibility response at a frequency f for a uniaxial thin film magnetized to saturation along the easy axis by a static external field H_{ext} may be written in the FMR form as[9,10]

$$\chi(f)=\left(\frac{|\gamma|\mu_0}{2\pi}\right)^2\frac{M_S(H_{\mathrm{ext}}+H_k+M_S)}{[f_{\mathrm{res}}^2-f(f-i\Delta f_{\mathrm{VNA}})]}. \tag{2}$$

In the above, M_S is the saturation magnetization, H_k is the uniaxial anisotropy field parameter, f_{res} is the resonance frequency, γ denotes the electron gyromagnetic ratio, and Δf_{VNA} is the frequency swept linewidth. The full fitting function to the data was written as

$$U_{\mathrm{fit}}(f)=C[1+\chi_0+\chi(f)e^{i\phi}], \tag{3}$$

where C is a real scaling parameter, χ_0 is a complex offset parameter, and ϕ is a phase shift adjustment.

The extracted data were fit simultaneously to both real and imaginary parts of the function $U_{\mathrm{fit}}(f)$ to obtain the f_{res} and Δf_{VNA} values. The form in Eq. (3) is based on the fact that $U(f)$ is related to the actual complex microwave permeability μ and that μ, in turn, is equal to $\mu_0[1+\chi(f)]$.

For the data shown in Fig. 4, the fitting procedure gives f_{res} and Δf_{VNA} values of 2.0 GHz and 236 ± 12 MHz, respectively. The fitted values for Re χ_0, Im χ_0, and ϕ for these particular data were $-157°$, $-34°$, and $24°$, respectively. As a demonstration that this procedure actually corresponds to a Lorentzian loss profile, the Fig. 4 inset shows the same data in a normalized loss format corresponding to $-\mathrm{Im}[\chi(f)]$, along with the theoretical response shown by the solid curve. The procedure gave satisfactory fits for the entire ensemble of VNA data. All FMR frequency fits were accurate to better than 1 MHz and the linewidth fits were accurate to 5%. For a given fit, the values for χ_0 were in the range expected from the tail of the reference field FMR $\chi(f)$ response. The fitted ϕ values were in the 21°–25° range. The data were not corrected for the waveguide width[11,12] since no significant influence was found on the linewidth.

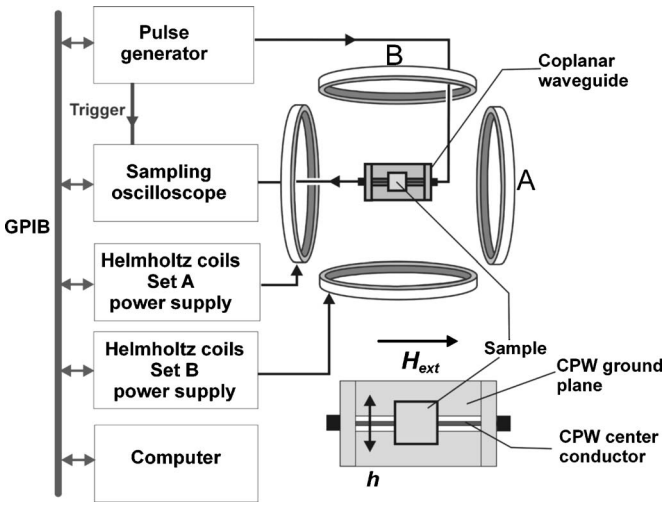

FIG. 5. Schematic diagram of the pulsed inductive microwave magnetometer. The sample is placed on the coplanar waveguide (CPW) structure, as indicated. The inset shows the field geometry and sample with respect to the center conductor and the ground plane of the coplanar waveguide, with the mutually perpendicular static applied field H_{ext} and the microwave field h in the plane of the film, as indicated.

C. The pulsed inductive microwave magnetometer technique

The pulsed inductive microwave magnetometer technique allows the user to obtain the loss parameters in the ferromagnetic material from the free induction decay of the dynamic magnetization in response to a pulsed magnetic field rather than a microwave field.[7,13] Figure 5 shows a simplified diagram of the PIMM system. The pulsed field h is provided by a CPW structure, with the thin film sample positioned across the center conductor as indicated. Two sets of Helmholtz coils provide the necessary static fields. Set A is used to produce the static field parallel to the CPW axis and perpendicular to the pulsed field for measurement. This field controls the ringing response. Set B is used to saturate the film in the transverse direction in order to obtain a reference signal without ringing. These responses are measured in the time domain with a 20 GHz sampling oscilloscope.

The data reported below were obtained for a range of static measurement fields from 1.6 to 8 kA/m (20 to 100 Oe). The CPW structure had a center strip width of 220 μm. The input CPW field pulses have a rise time and duration of 50 ps and 10 ns, respectively. The maximum pulse field amplitude was approximately 64 A/m (0.8 Oe). This combination of static and pulsed field amplitudes ensured a linear response.[14] The Permalloy film samples were placed on the top of the CPW structure with the substrate side down in order to minimize any possible impedance mismatch due to the presence of the sample. The films were oriented with the uniaxial anisotropy easy axis parallel to the

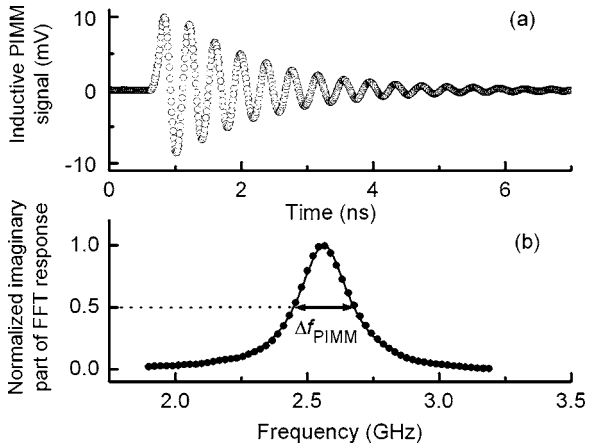

FIG. 6. Representative data from the pulsed inductive microwave magnetometer (PIMM) system. Graph (a) shows the inductive signal for film S50A with a static applied field of 5.3 kA/m (66 Oe). Graph (b) shows the imaginary part of the fast Fourier transform (FFT) of the signal in (a). The solid curve in (b) is a Lorentzian fit to the data.

CPW line. The dynamic magnetization ringing response to the initial step in the CPW field pulse was measured and used for the decay and linewidth analyses.

A given dynamic magnetization response to the initial step in the CPW pulsed field $h(t)$ is measured and analyzed in four steps. (1) A static transverse field H_B (coil set B) of 5.6 kA/m (70 Oe) is first applied to saturate the film in the hard direction. (2) With H_B reset to zero, the desired easy direction static field H_A (coil set A) is applied, the $h(t)$ step is applied, and the output voltage versus time profile from the CPW line, taken as $V_A(t)$, is measured for a range of times from about 0.5 ns prior to the onset of the step pulse to 10 ns after the step. (3) With H_A reset to zero and H_B held at 5.6 kA/m (70 Oe), $h(t)$ is again applied and a second output voltage versus time profile, $V_B(t)$, is measured again to provide a reference data set. The step response was then obtained as $V_R(t)=V_A(t)-V_B(t)$. (4) A fast Fourier transform of this time domain ringing response signal is then used to extract absorption and dispersion versus frequency profiles. Fits of these FFT data to a standard damped oscillator frequency response then yield the FMR frequency and FWHM frequency linewidth at each measurement field.

Figure 6 shows representative data for sample S50A. These data are for a measurement field of 5.3 kA/m (66 Oe). Figure 6(a) shows the free induction decay $V_R(t)$ response discussed above. In Fig. 6(b), the loss component of the FFT response and a Lorentzian fit to those data are shown by the open circles and the solid curve, respectively. The corresponding resonance frequency f_{res} is 2.53 ± 0.05 GHz, and the fitted FWHM frequency linewidth Δf_{PIMM} for the profile in (b) is 236 ± 11 MHz.

III. FIELD AND FREQUENCY SWEPT LINEWIDTH CONNECTIONS

The FMR linewidth is a measure of the microwave loss properties of the sample. The SL-FMR technique yields field swept FMR linewidths at a fixed frequency, whereas the VNA-FMR and PIMM techniques give frequency swept linewidths at fixed fields. How can one ascertain whether these different linewidths at different types of operating points give an equivalent loss? One way to do this is to use the FMR frequency versus field relation to convert between these two types of linewidths, cast all linewidths into one or the other of these formats, and then compare the results.

For a magnetic thin film with an in-plane uniaxial anisotropy and magnetized to saturation along the easy axis by a static external field H_{ext}, the Kittel FMR frequency f_{Kittel} may be written as

$$f_{Kittel}(H_{ext}) = \frac{|\gamma|}{2\pi}\mu_0\sqrt{(H_{ext}+H_k)(H_{ext}+H_k+M_S)}. \quad (4)$$

The inverse connection for the Kittel FMR field $H_{Kittel}(f)$ for a given operating point frequency f may be obtained from Eq. (4) by letting $f_{Kittel}(H_{ext})$ go to f, letting H_{ext} go to $H_{Kittel}(f)$, and solving for H_{Kittel}. It is well established that the FMR peak positions in the field or frequency obtained from all three methods conform with Eq. (4).

It is clear from Eq. (4) that the FMR field and the FMR frequency do not scale linearly with each other. This nonlinear scaling is closely connected to the ellipticity of the FMR precession cone given by the square root of the ratio of the two factors inside the square root in Eq. (4). This ellipticity also leads to a nonlinear connection between the field swept linewidth ΔH for a given frequency f and resonance field $H_{Kittel}(f)$ and the corresponding frequency swept linewidth Δf for a given field H_{ext} and resonance frequency $f_{Kittel}(H_{ext})=f$. If the linewidths are relatively small, relative to the FMR field or frequency, one can use Eq. (4) and a simple differentiation to obtain field swept and frequency swept linewidth connections as

$$\Delta f = \Delta H \left.\frac{\partial f_{Kittel}(H_{ext})}{\partial H_{ext}}\right|_{H_{ext}=H_{Kittel}(f)} = |\gamma| P_A(f) \Delta H \quad (5)$$

and

$$\Delta H = \Delta f \left.\frac{\partial H_{Kittel}(f)}{\partial f}\right|_{f=f_{Kittel}(H_{ext})} = \frac{\Delta f}{|\gamma| P_A(f)}. \quad (6)$$

This type of conversion has been discussed by Patton[1,9] and most recently by Kuanr *et al.*[15] These relations will be used to convert the SL-FMR linewidths in field to equivalent frequency linewidths and the VNA-FMR and PIMM linewidths in frequency to equivalent field linewidths for the comparisons given in the next section. The dimensionless $P_A(f)$ factor defined above provides a convenient way to account for the ellipticity of the FMR response in relaxation rate and linewidth analyses.[16] For an in-plane magnetized film, the $P_A(f)$ function is reduced to the simple form

$$P_A(f) = \sqrt{1+\left(\frac{|\gamma|\mu_0 M_s}{4\pi f}\right)^2}. \quad (7)$$

This function will be important for the frequency linewidth discussion below.

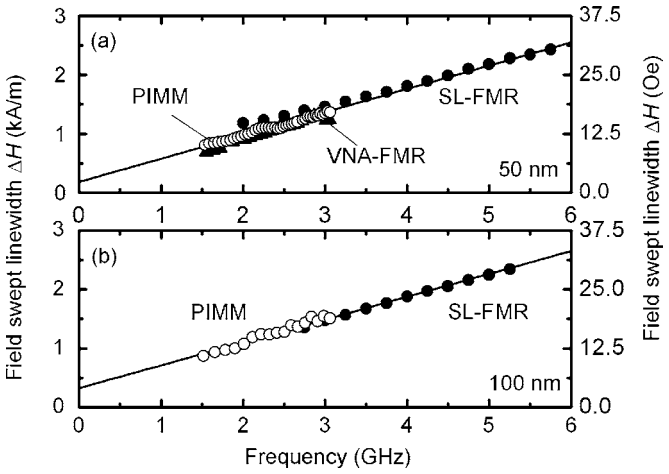

FIG. 7. Comparison of the field format linewidth ΔH results obtained from the stripline, the vector network analyzer, and PIMM techniques on the 50 and 100 nm films. The solid circles are the SL-FMR results, the solid triangles are the VNA-FMR results, and the open circles are the PIMM results. The solid lines are linear fits to all the points. Graph (a) shows the ΔH values vs frequency for the films S50A and S50B, and graph (b) shows the ΔH values vs frequency for sample S100.

IV. SL-FMR, VNA-FMR, AND PIMM LINEWIDTH COMPARISONS

Figures 7 and 8 show linewidth comparison results in field linewidth versus frequency and frequency linewidth versus frequency formats, respectively. Figures 7(a) and 8(a) in each case correspond to SL-FMR and PIMM data on sample S50A and to VNA-FMR data on sample S50B. Figures 7(b) and 8(b) correspond to SL-FMR and PIMM data on sample S100. The SL-FMR, VNA-FMR, and PIMM results are shown by solid circles, solid triangles, and open circles, respectively. The linewidth conversions were based on nominal free electron $|\gamma|/2\pi$ and H_k values of 28 GHz/T and 480 A/m (6 Oe), respectively, and the $\mu_0 M_S$ value of 1.055 T.[17] These values are consistent with the FMR frequency versus field data for the three samples. Error bars for each data set are on the order of the size of the data points. The straight lines show fits for the full (a) and (b) data sets in Fig. 7. The corresponding slopes and intercepts are useful parameters for comparison with typical Permalloy data in the literature.[18,19] These lines carry over to the curves shown in Fig. 8.

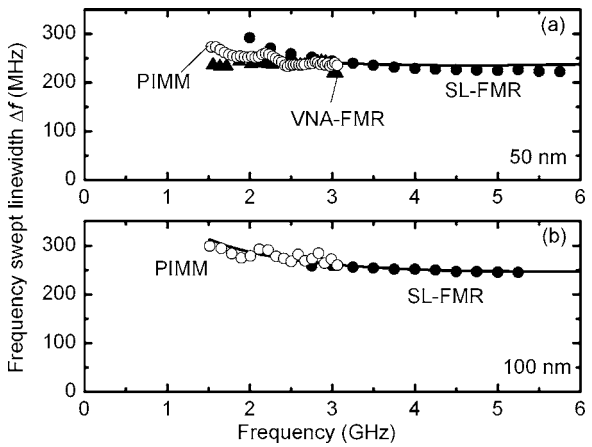

FIG. 8. Comparison of the frequency format linewidth Δf results obtained from the stripline, the vector network analyzer, and PIMM techniques on the 50 and 100 nm films. The solid circles are the SL-FMR results, the solid triangles are the VNA-FMR results, and the open circles are the PIMM results. The solid curves are the corresponding fits to the lines in Fig. 7. Graph (a) shows the Δf values vs frequency for the films S50A and S50B, and graph (b) shows the Δf values vs frequency for sample S100.

The field linewidth versus frequency data in Fig. 7 show consistent results from method to method. The fitted slopes for the straight lines in (a) and (b) are 393 ± 8 A/m/GHz (4.85 ± 0.1 Oe/GHz) and 385 ± 24 A/m/GHz (4.9 ± 0.3 Oe/GHz), respectively. The corresponding intercepts for the straight line fits are $183\pm24(2.3\pm0.3)$ and 326 ± 16 A/m (4.1 ± 0.2 Oe), respectively. The regression coefficients for the fits shown in (a) and (b) are 0.989 and 0.995, respectively. This type of linewidth versus frequency response is similar to that found in many previous FMR experiments on Permalloy and other metal ferromagnetic films.[18–24]

Such linewidth responses are often interpreted in terms of a combined inhomogeneous broadening and Landau-Lifshitz or Gilbert damping model.[19,22] Within this framework, one would expect a field swept half power linewidth of the form

$$\Delta H = \Delta H_0 + \frac{4\pi\alpha f}{|\gamma|}, \tag{8}$$

where ΔH_0 is a measure of the inhomogeneous broadening in a field that affects the FMR response and α is the Landau-Lifshitz or Gilbert damping parameter in a dimensionless form. For low linewidths, as found here, the Landau-Lifshitz and Gilbert models are equivalent for all practical purposes. The slopes given above correspond to α values of about 0.007 for both the 50 and 100 nm films. These are typical α values for low loss metal films.[18–21,23,24] Intercept ΔH_0 values in the few tenths of kA/m range are also consistent with the expected field inhomogeneities due to anisotropy dispersion and other effects.[19,20,25] It is to be emphasized that the focus of this paper is on measurements and measurement comparisons, and not on the physical origins of the linewidth versus field or frequency response. The interpretation of these responses continues to be a subject of intense study.

Similar comments apply to the frequency linewidth versus frequency presentations in Fig. 8. The data for the three techniques are consistent from method to method. The change of format expands the scatter in the data from the fit line at low frequencies. This can be made clear from the linewidth conversion formulas established above. Based on Eqs. (5), (7), and (8), one can write

$$\Delta f = (|\gamma|\Delta H_0 + 4\pi\alpha f)\sqrt{1+\left(\frac{|\gamma|\mu_0 M_s}{4\pi f}\right)^2}. \tag{9}$$

For Permalloy, with $|\gamma|\mu_0 M_s/2\pi \approx 28$ GHz, the $P_A(f)$ conversion amounts to a $|\gamma|\mu_0 M_s/4\pi f$ multiplier. This results in an increase in the frequency linewidth, relative to $|\gamma|\Delta H$, as well as any corresponding scatter, for frequencies below 3 GHz or so. The ΔH_0 intercept in the field linewidth versus frequency data presentation format corresponds to the upward curvature of the Δf versus f response in Fig. 8. How-

ever, work in progress indicates that there may be additional contributions to this curvature for frequencies below the 1.5 GHz limit of the data reported here. The leveling off in Δf for $f > 3$ GHz or so corresponds to the dominance of the $4\pi\alpha f$ term relative to the zero frequency $|\gamma|\Delta H_0$ term in Eq. (9). In this limit, the theoretical Δf is just $\alpha|\gamma|\mu_0 M_s$.

ACKNOWLEDGMENTS

The Colorado State University contribution to this work was supported by the National Science Foundation (Grant No. DMR-0108797) the U.S. Army Research Office (Grants Nos. DAAD19-02-1-0197 and W911NF-04-1-0247) and the Information Storage Industry Consortium (INSIC) Ultra High Density Recording (EHDR) program.

[1] C. E. Patton, J. Appl. Phys. **39**, 3060 (1968).
[2] J. J. Green and T. Kohane, SCP Solid State Technol. **7**, 46 (1964).
[3] I. Bady, IEEE Trans. Magn. **3**, 521 (1967).
[4] F. J. Cadieu, R. Rani, W. Mendoza, B. Peng, S. A. Shaheen, M. J. Hurben, and C. E. Patton, J. Appl. Phys. **81**, 4801 (1997).
[5] W. Barry, IEEE Trans. Microwave Theory Tech. **MTT-34**, 80 (1986).
[6] A. B. Kos, T. J. Silva, and P. Kabos, Rev. Sci. Instrum. **73**, 3563 (2002).
[7] T. J. Silva, C. S. Lee, T. M. Crawford, and C. T. Rogers, J. Appl. Phys. **85**, 7849 (1999).
[8] P. Wolf, J. Appl. Phys. **32**, 95S (1961).
[9] C. E. Patton, in *Magnetic Oxides*, edited by D. J. Craik (Wiley, London, 1975), pp. 575–645.
[10] See, for example, D. Stancil, *Theory of Magnetostatic Waves* (Springer-Verlag, New York, 1993); P. Kabos and V. S. Stalmachov, *Magnetostatic Waves and their Applications* (Chapman & Hall, London, 1994).
[11] G. Counil, J.-V. Kim, T. Devolder, C. Chappert, K. Shigeto, and Y. Otani, J. Appl. Phys. **95**, 5646 (2004).
[12] M. L. Schneider, T. Gerrits, A. B. Kos, and T. J. Silva, Appl. Phys. Lett. **87**, 072509 (2005).
[13] C. Alexander, J. Rantschler, T. J. Silva, and P. Kabos, J. Appl. Phys. **87**, 6633 (2000).
[14] J. P. Nibarger, R. Lopusnik, and T. J. Silva, Appl. Phys. Lett. **82**, 2112 (2003).
[15] B. Kuanr, R. Camley, and Z. Celinski, Appl. Phys. Lett. **87**, 012502 (2005).
[16] V. Kambersky and C. E. Patton, Phys. Rev. B **11**, 2668 (1975).
[17] J. P. Nibarger, R. Lopusnik, Z. Celinski, and T. J. Silva, Appl. Phys. Lett. **83**, 93 (2003).
[18] C. E. Patton and C. H. Wilts, J. Appl. Phys. **38**, 3537 (1967).
[19] B. Heinrich, J. F. Cochran, and R. Hasegawa, J. Appl. Phys. **57**, 3690 (1985).
[20] J. J. Krebs, F. J. Rachford, P. Lubitz, and G. A. Prinz, J. Appl. Phys. **53**, 8058 (1982).
[21] R. Urban, G. Woltersdorf, and B. Heinrich, Phys. Rev. Lett. **87**, 217204 (2001).
[22] X. Liu, J. O. Rantschler, C. Alexander, and G. Zangari, IEEE Trans. Magn. **39**, 2362 (2003).
[23] D. J. Twisselmann and R. D. McMichael, J. Appl. Phys. **93**, 6903 (2003).
[24] Z. Celinski and B. Heinrich, J. Appl. Phys. **70**, 5935 (1991).
[25] J. O. Rantschler and C. Alexander, J. Appl. Phys. **93**, 6665 (2003).